Alma Mater Studiorum Università di Bologna
Archivio istituzionale della ricerca

Multi-Band Measurements for Deep Learning-Based Dynamic Channel Prediction and Simulation

24 November 2024

This is the final peer-reviewed accepted manuscript of:

Multi-band High-Mobility Measurements for Deep Learning-based Channel Prediction and Simulation

Faruk Pasic*, Nicola Di Cicco†, Marco Skocaj‡, Massimo Tornatore†, Stefan Schwarz*,
Christoph F. Mecklenbräuker* and Vittorio Degli-Esposti‡
*Institute of Telecommunications, TU Wien, Austria
†DEIB, Politecnico di Milano, Italy
‡DEI, University of Bologna, & WiLab, CNIT, Italy
faruk.pasic@tuwien.ac.at, nicola.dicicco@polimi.it

Abstract—Next-generation mobile communication systems support millimeter Wave (mmWave) transmission and high-mobility scenarios. To cope with propagation environments with unprecedented challenges, data-driven methodologies such as Machine Learning (ML) are expected to act as a fundamental tool for decision support in future mobile systems. However, high-quality measurement datasets need to be made available to the research community in order to develop and benchmark ML-based methodologies for next-generation wireless networks. We present a reliable testbed for collecting channel measurements at sub-6 GHz and mmWave frequencies. Further, we describe a rich dataset collected using the presented testbed. Our public dataset enables the development and testing of innovative ML-based channel models for both sub-6 GHz and mmWave bands on real-world data. We conclude this paper by discussing promising experimental results on two illustrative ML tasks leveraging on our dataset, namely, channel impulse response forecasting and synthetic channel transfer function generation, upon which we propose future exploratory research directions.

Index Terms—machine learning, deep learning, radio channel prediction, radio channel simulation, vehicular communications, channel sounding, channel measurements.

I. INTRODUCTION

Adaptive wireless transmission is among the core paradigms for achieving consistent communication performance close to the Shannon limit [1]. In particular, to estimate the quality of a radio link and to adapt the transmission parameters to the current channel condition, the transmitter needs to know the Channel State Information at the Transmitter (CSIT), i.e., a set of channel properties of the radio link. These properties are strongly affected by several propagation phenomena such as path loss, scattering, fading and shadowing [2]. Accurate CSIT knowledge allows optimally tuning several transmission parameters e.g., the transmit power, constellation size, coding rate, single- and multiuser-beamforming/precoding, as well as scheduling and resource allocation. Whenever link adaptation is based on the assumption of instantaneous CSIT, outdated CSIT can cause significant performance degradation [3]. For example, feedback delay and processing delay in frequency-division duplex (FDD) and time-division duplex (TDD) systems, respectively, are causes of outdated CSIT. Both feedback

and processing delays become more severe in rapidly changing fading channels.

To deal with the problem of outdated CSIT in a data-driven way, researchers have already proposed several channel prediction methods based on ML. The goal of channel prediction is to accurately forecast future CSIT in advance with a time span that counteracts the induced delay. The proposed methods are mostly based on Recurrent Neural Networks (RNN), as they are especially suited for processing time-series data [4]. For example, in [5], authors develop a channel forecaster based on Long Short-Term Memory (LSTM) and Gated Recurrent Unit (GRU) neural network layers.

In this context, next-generation mobile communication systems are planned to support mmWave transmission and are expected to operate in high-mobility scenarios (e.g., vehicular and high-speed train). Due to much faster channel fading, abrupt shadowing transitions and larger Doppler spreads, high-mobility channel prediction poses a significant challenge. Therefore, high-quality datasets of channel measurements in high-speed scenarios are required for benchmarking ML-based techniques in real-world conditions.

However, collecting reliable and self-consistent datasets of comparative measurements between sub-6 GHz and mmWave bands is not trivial. For example, sub-6 GHz and mmWave antennas cannot be placed at the same position at the same time, due to mechanical constraints. Therefore, one would need to perform measurements at different times if we want to conduct measurements over the same measured trace. This effect may result in different small-scale fading and fast-fading behavior for different frequency bands. Hence, a fair comparison between sub-6 GHz and mmWave bands is altered.

In this paper, to address these multifaceted challenges, we provide the research community with a reliable and rich high-speed channel measurements dataset for sub-6 GHz and mmWave frequencies, and we illustrate its potential application for ML-based channel forecasting and simulation. Our contributions are summarized as follows:

- We present the testbed hardware [6] to enable a fair comparison between sub-6 GHz and mmWave systems in terms of small-scale and fast-fading in a high-mobility environment.
- We describe a methodology that allows channel sounding over the identical measured antenna trace with the same
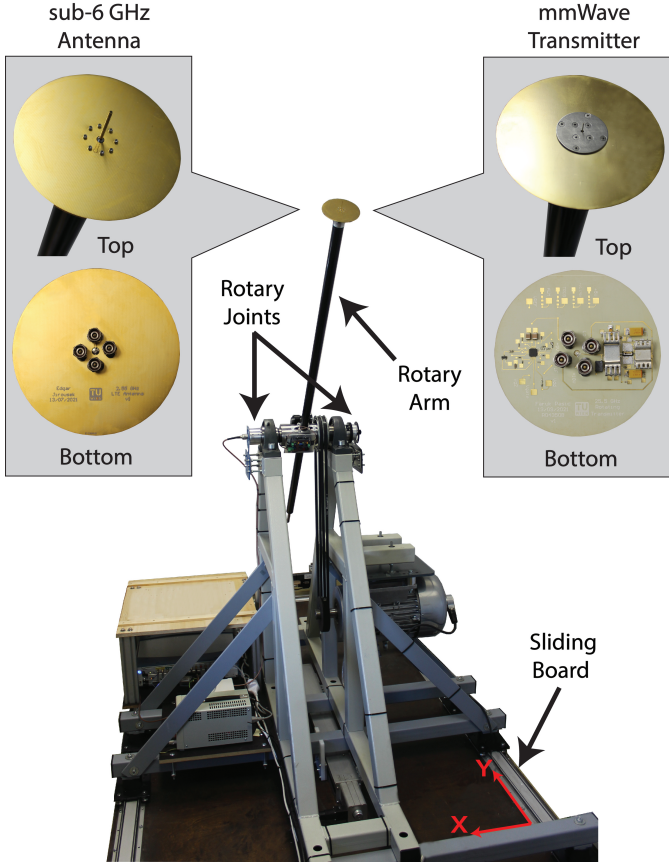

F. Pasic and N. Di Cicco are first co-authors of this paper.

Fig. 1. The testbed setup to compare sub-6 GHz and mmWave in a high-mobility environment. A sub-6 GHz or mmWave Tx antenna is mounted at the end of the rotary arm.

controlled velocity, but at different frequency bands.

- We provide the measurement dataset obtained by conducting channel measurements at sub-6 GHz (2.55 GHz) and mmWave (25.5 GHz) bands and at velocities of 40 km/h and 100 km/h.
- We present two illustrative use cases of our dataset for the application of ML-based techniques: RNN-based channel forecasting and Generative Adversarial Network-based channel impulse response (CIR) simulation.

II. TESTBED DESIGN AND IMPLEMENTATION

In this section, we provide a detailed description of the proposed testbed. We focus on the testbed implementation for sub-6 GHz and mmWave cases, as well as on the necessary time and frequency synchronization. Then, we elaborate on the two major advantages of the proposed testbed: reproducibility and controllability. Finally, we introduce a methodology for ensuring a fair comparison between measurements performed at different frequency bands and different velocities.

A. Testbed Hardware

Our testbed setup consists of a moving transmitter and a static receiver placed in an indoor laboratory environment [7]. Our moving transmitter is based on a rotary unit described

in [8]. This rotary unit spins a transmit antenna around a central axis up to 1000 rotations per minute (rpm).

Specifically, the transmit antenna is mounted on a rotating aluminum alloy arm with a length of 1 m and can thereby reach constant but adjustable velocities up to 400 km/h. The speed of the rotary arm is controlled through an RS-485 connection using an off-the-shelf frequency inverter.

Furthermore, the rotary unit is equipped with rotary joints at each end of the central axis. These rotary joints are required to connect the two rotating coaxial cables in the arm to the static cables and the signal source outside the arm. Except for the rotation, the cables themselves are glued inside the arm and therefore static to not change their electrical properties due to bending. The maximum allowed signal frequency for these rotary joints is 12.4 GHz. Therefore, sub-6 GHz signals can be directly transmitted to the end of the rotary arm, but mmWave signals cannot. To our best knowledge, a rotary joint capable of both mmWave transmission and rotation up to approximately 1000 rpm is not available off-the-shelf. Therefore, the testbed setup requires hardware modifications to enable mmWave transmissions.

In the following, for both sub-6 GHz and mmWave cases, the transmit signal is generated with an Arbitrary Waveform Generator (AWG) (Keysight M8195A) and the received signal is sampled with a signal analyzer (Rohde & Schwarz FSW67).

B. Sub-6 GHz Setup

In the sub-6 GHz case, the transmit Intermediate Frequency (IF) signal is generated offline using Python, and is digitally up-converted to the center frequency of 2.55 GHz by the AWG. The up-converted signal is then fed through the rotary joint to the end of the rotary arm. Finally, the signal is radiated by a self-built 2.55 GHz monopole antenna (see Fig. 1).

C. Millimeter Wave Setup

In the mmWave case, as previously mentioned, a direct transmission of the Radio Frequency (RF) signal through the rotary joint is not possible. Therefore, we perform a frequency up-conversion by means of a mmWave transmitter at the end of the arm. During the rotation, the end of the rotary arm is exposed to significant acceleration forces. Thus, the mmWave transmitter needs to be lightweight. Therefore, using commercially available, bulky RF modules with connectors is not feasible. As a possible solution, we developed our mmWave transmitter on a 6-layered Printed Circuit Board (PCB) with the RF dielectric substrate Rogers RO4350B. The PCB consists of Surface Mount Device (SMD) components on the bottom side and a monopole antenna with a ground plane on the top side (see Fig. 1). The mmWave transmitter consists of an up-converter, a bandpass filter, a power amplifier and the monopole antenna. The entire PCB has a remarkably lightweight design, weighing only 43.1 gramms.

As before, the IF signal is generated offline using Python and digitally up-converted to the center frequency of 5.5 GHz by the AWG. Moreover, the mmWave transmitter requires a Local Oscillator (LO) tone to perform the up-conversion of the IF signal to a RF range. The LO tone at 10 GHz is generated

with a Continuous Wave (CW) signal generator (R&S SMF). We use one single-channel rotary joint to transmit the IF signal and the other rotary joint to transmit the LO signal to the mmWave transmitter placed at the end of the rotary arm.

Other than the IF and LO signals, the mmWave transmitter requires a $+5\,\text{V}$ and a $+10.175\,\text{V}$ DC power supply. Since both rotary joints have already been utilized for high-frequency signals, there are no rotary joints left to transmit the DC supply during the rotation. As a possible solution, we mounted a battery power supply on the central rotating axis, such that it is exposed to small acceleration forces only.

Within the mmWave transmitter, the up-converter Integrated Circuit (IC) performs LO frequency doubling. The doubled LO frequency mixed with the IF signal leads to an RF frequency of $25.5\,\text{GHz}$. As the up-converter, we utilize the Macom MAMF-011024 which operates in the frequency range from 21 to $27\,\text{GHz}$. Besides the desired RF signal at $25.5\,\text{GHz}$, the up-converter generates additional spectral components such as higher-order harmonics and intermodulation products. To suppress these unwanted components, we use a $25-26\,\text{GHz}$ band-pass filter (B259MC1S). Another drawback of the up-converter is the low output power level, which cannot overcome the large path loss at mmWave frequencies. Therefore, we leverage on a power amplifier (HMC994APM5E) for increasing the transmit power level. Finally, the amplified mmWave signal is radiated by the self-built $25.5\,\text{GHz}$ monopole antenna.

For performing a fair comparison between sub-6 GHz and the mmWave, we require the same receive antenna for both scenarios. Therefore, we employ $2.55\,\text{GHz}$ and $25.5\,\text{GHz}$ horn antennas with the same opening angle as receive antennas for sub-6 GHz and mmWave, respectively.

D. Synchronization

To reach optimum performance of the proposed channel sounding system, accurate frequency and timing synchronization are required. In a typical vehicular drive-by measurement setup, the transmitter and the receiver are located far away from each other [9], hence a cable connection for providing precise frequency and timing synchronization is not feasible. Instead, to provide precise frequency synchronization, expensive Rubidium frequency standards are usually employed at the transmitter and the receiver [9]. As a possible solution for precise timing synchronization, a preamble with good auto-correlation properties is often exploited to find the beginning of the received channel-sounding signal [10].

In the proposed setup, the transmitter and the receiver are placed only $10\,\text{m}$ apart in the indoor laboratory environment. Therefore, the cable connection is feasible and it represents a significant advantage of the proposed setup compared to usual drive-by ones. To provide accurate frequency synchronization, we interconnect the AWG at the transmitter's site and the signal analyzer at the receiver's site with a $100\,\text{MHz}$ reference. The same applies to time synchronization. The rotary unit is equipped with a trigger unit based on a Field Programmable Gate Array (FPGA) and a rotational encoder. The signal of the rotational encoder is decoded by a counter and a comparator to form a trigger signal. The trigger signal is thereafter fed

through cables to the arbitrary waveform generator at the transmitter and the signal analyzer at the receiver. Thereby, it is possible to repeatably trigger a measurement at a precisely defined position of a rotary arm once per revolution.

E. Reproducibility and Controllability

Two major advantages of the proposed testbed setup are reproducibility and controllability. Reproducibility is the ability to repeat a measurement sample under equal channel conditions. The reproducibility can hardly be achieved in real-world drive-by measurements. More precisely, the surroundings (moving vehicles and pedestrians) are extremely unlikely to remain constant over time and it is also very difficult to drive exactly the same route twice by car. Our testbed setup achieves reproducibility in the following way. Firstly, we keep the fading environment static by ensuring that there are no people or moving objects within the room during a measurement campaign. This enables us to observe the effect of a single system parameter (e.g., velocity, Tx power) without influence of the other ones. Secondly, using the trigger unit, we ensure that the transmit antenna moves over an identical circular trace with the same constant velocity, but at different frequencies. Thirdly, we keep the receive antenna static on a laboratory table in the neighboring room. Thereby, we allow a direct comparison of the measured wireless channel in terms of fading environment and channel statistics.

The second major advantage of our proposed setup is controllability, i.e., the ability to control environmental and system parameters. In our setup, we can easily change the average signal-to-noise ratio (SNR) by adjusting the transmit power and change the velocity by adjusting the rotation speed through the frequency inverter.

F. Ensuring Fair Comparisons

To fairly compare measurements performed at different frequency bands and different velocities, we extend the methodology proposed in [7]. Firstly, we have to keep the fading environment static. To this end, the measurement campaign has been conducted within 2 hours with no people or moving objects within the room during the measurements. Secondly, we have to ensure transmitting the same number of channel sounding symbols along the same measured trace for different velocities. As a possible solution, we adjust the symbol duration to the transmitter's velocity. Specifically, we choose a short symbol duration for high-velocity measurements and a long symbol duration for low-velocity measurements. Such a selection of parameters makes the measurement results independent of the transmitter's velocity and therefore leads to a fair comparison.

III. DATASET

In this section, we first describe our measurement campaign with all measured scenarios and explain the post-processing procedure of the measurement results to obtain our dataset. Subsequently, we show some examples of data extraction and provide practical guidelines the use of our dataset.
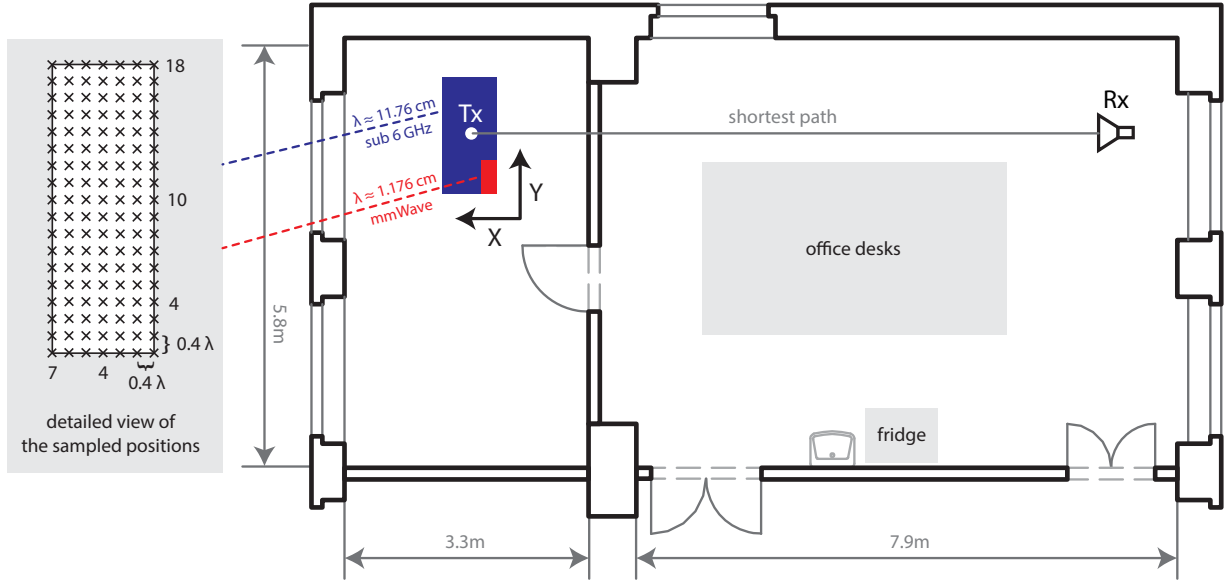
Fig. 2. Measured indoor laboratory environment. The rotating transmitter and the statical receiver are located in neighboring rooms. The transmitter is placed on a sliding board, which is moved according to the illustrated rectangular grid for both sub-6 GHz and mmWave.
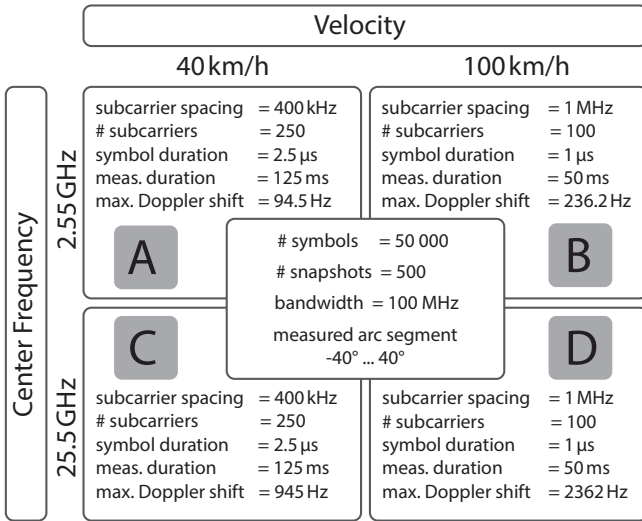

Fig. 3. Considered measurement parametrization. The wireless channel is measured over an identical antenna trace for all measured scenarios.

A. Measurement Campaign

Using the above described testbed and methodology, we perform channel sounding measurements in a controlled indoor environment as shown in Fig. 2. We conduct measurements of all four combinations of low (40 km/h) or high (100 km/h) speed and sub-6 GHz (2.55 GHz) or mmWave (25.5 GHz) center frequency, with parameters provided in Fig. 3. The transmit antenna moves along the same trace (circular arc segment) at the rotary arm with a constant velocity, while the receive antenna is static on a laboratory table in the neighboring room.

We use an Orthogonal Frequency-Division Multiplexing (OFDM) signal as a transmit signal. To keep the peak-to-average power ratio (PAPR) low, the transmit signal is designed using a Zadoff-Chu sequence [11]. We transmit a measurement sequence of 50 000 identical OFDM symbols (500 snapshots of 100 symbols each) as channel sounding signal. The measurement sequence is grouped into 500 snapshots of 100 symbols each. This grouping is made under the assumption that the wireless channel between the moving antenna and the static receiver is constant in time for the duration of one snapshot. The trigger unit initiates the transmission when the rotating arm passes an angular position of $-40°$. The transmission continues as the rotating antenna moves along the trace (arc segment) from $-40°$ to $40°$. We choose a high subcarrier spacing of 1 MHz for high-velocity measurements and a low subcarrier spacing of 400 kHz for low-velocity measurements. As previously explained, we thereby achieve comparability of measurement results.

At the receiver side, we exploit the first OFDM symbol of each snapshot as a cyclic prefix to eliminate intersymbol interference (ISI). We discard the first OFDM symbol of each snapshot and perform averaging of the remaining 99 symbols to improve the Signal-to-Noise Ratio (SNR) by approximately 20 dB. After OFDM processing, we estimate the wireless channel via least-squares estimation for all subcarriers. In this way, we obtain a time-variant channel transfer function for discrete-time (snapshots) and frequency (subcarriers) as the final result of our measurement campaign.

Using this measurement procedure, we generate a dataset consisting of different time-variant channel transfer functions. These functions are generated by conducting measurements at different positions of the transmitter. In addition to the rotating in a single position, the transmitter can also be moved in space. The transmitter (the rotary unit) is placed on a sliding board, which can be moved by 81 centimeters along the x-axis and by 33 centimeters along the y-axis. We assume that the channel is locally stationary within a window of approximately six wavelengths of motion. For 2.55 GHz and 25.5 GHz, a
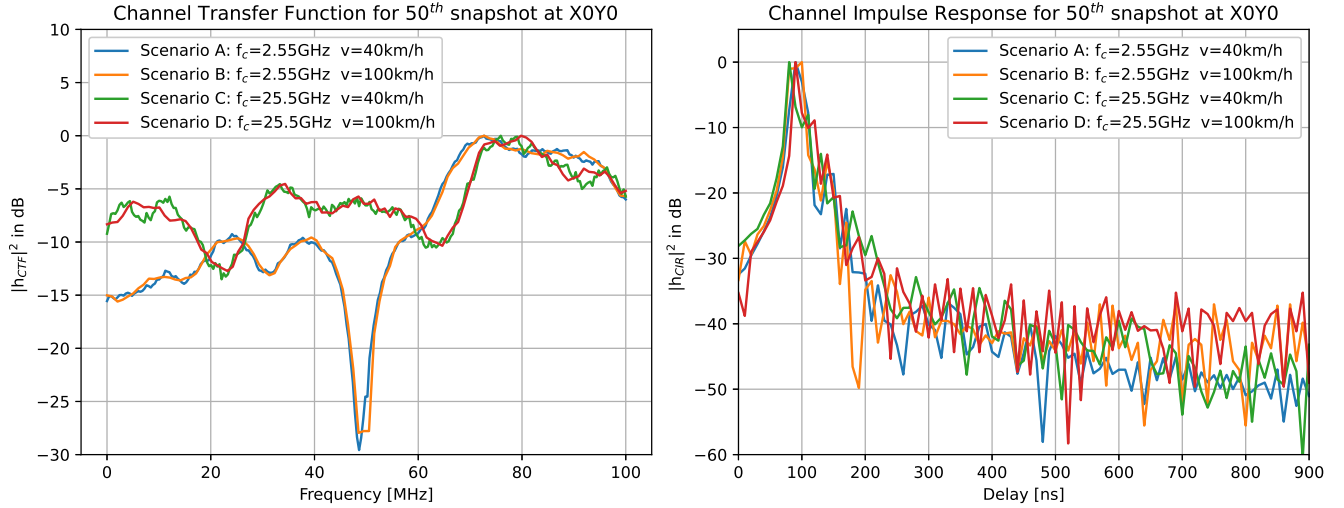
Fig. 4. Channel transfer function and channel impulse response of the 50th snapshot in all of the measured scenarios. Location on the x-y axis is X0Y0.

window of six wavelengths corresponds to approximately 70 cm and approximately 0.7 cm, respectively. Considering these stationarity assumptions, we performed measurements at 126 different positions according to the rectangular grid shown in Fig. 2. The positions on the x- and y-axis are mutually separated by 0.4 λ. The blue (large) and red (small) rectangles indicate the measured region for sub-6 GHz and mmWave, respectively. Thereby, we obtain different realizations of the same wireless channel for both sub-6 GHz and mmWave.

B. Dataset Description

The dataset is placed on IEEE DataPort [12], and consists of time-varying channel transfer functions classified in four categories depending on the measurement scenarios from Fig. 3. The dataset entries are given as complex-valued numpy (.npy) files in which rows and columns represent different snapshots and subcarriers, respectively. For each scenario, there are 126 channel realizations obtained by conducting measurements at different positions according to the rectangular grid shown in Fig. 2. Each name in the dataset is given in the format "frequency_velocity_position". For example, the entry "25_5GHz_100kmh_X6Y2.npy" denotes the time-varying channel transfer function measured at 25.5 GHz at the velocity of 100 km/h for the position six on the x-axis and position two on the y-axis.

In addition to the data files, an example Python file called "example.py" is provided. The example file extracts dataset entries based on the chosen input parameters, such as scenario, x- and y-position within the rectangular grid. As a result, the example file shows the channel transfer function (CTF) and the channel impulse response (CIR) for the selected parameters. The CIR is obtained by performing Inverse Fast Fourier Transform (IFFT) of the CTF over subcarriers. In Fig. 4, we show the CTF and CIR for the 50$^{\text{th}}$ snapshot and positions X0Y0 for all measured scenarios.

IV. ILLUSTRATIVE MACHINE LEARNING USE-CASES AND EXPLORATORY RESEARCH DIRECTIONS

In this Section, we outline two illustrative ML use-cases for the presented dataset, namely i) CIR forecasting using recurrent neural networks, and ii) CTF simulation using generative neural networks. For each task we describe a baseline ML approach, we discuss our main results, and we propose future research directions.

A. Channel Forecasting with Recurrent Neural Networks

We consider the problem of forecasting CIR values over a time horizon, given a time-series of past CIRs. In the context of an adaptive transmission systems, accurate CTF forecasting can help mitigating the problem of outdated CSIT in the presence of fast fading [5].

To implement our forecaster we leverage Long Term Short Memory (LSTM) neural networks with Variational Dropout. LSTM networks can efficiently learn complex temporal dependencies in the sequence of input CIR. Variational Dropout allows to estimate the uncertainty associated with each forecast, providing richer information for proactive decision-making.

Our channel forecaster is implemented as a classical encoder-decoder architecture, which comprises an encoder neural network and a decoder neural network. More specifically, the encoder and decoder networks consist of multiple LSTM layers with Variational Dropout [13]. The task of the encoder is to produce a fixed-dimension feature vector given an input time-series. The decoder takes as an input the context vector and the last CIR value, and outputs a forecast for the CIR value at the next time instant as well as an updated context vector. The forecasted CIR value and the updated context vector are recursively fed back to the decoder, and the process is repeated until the desidered forecast time-horizon is reached.

As an illustrative task, we will consider forecasting the absolute CIR values for a single subcarrier, i.e., we limit ourselves to a simple univariate forecasting problem. In particular, we
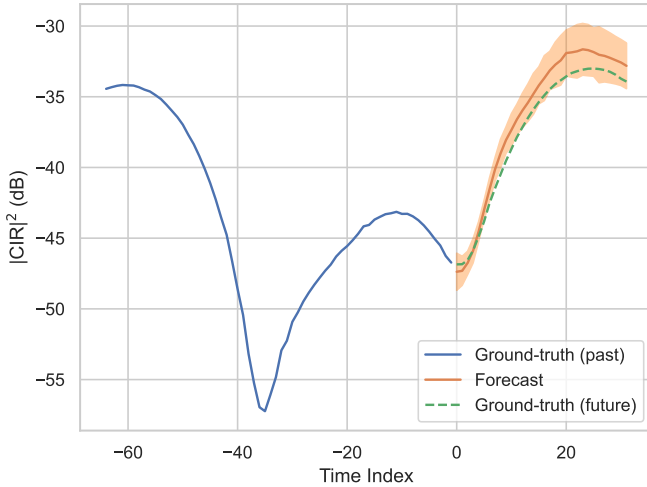
Fig. 5. Illustrative CIR mean forecasts and 95% confidence bands for a single OFDM subcarrier, 2.55GHz center frequency and 40km/h transmitter speed.

(a) Absolute CTF values from real measurements

(b) Absolute CTF measurements generated by a DCGAN

Fig. 6. Illustrative real and synthetic absolute CTF values for 2.55GHz center frequency and 40km/h speed. Time/frequency are the horizontal/vertical axes.

train our neural network to predict the future 32 CIR snapshots given 64 past CIR snapshots.

Fig. 5 shows an illustrative CIR forecast for 2.55GHz center frequency and 40km/h speed. Our encoder-decoder model correctly captured the CIR time-varying behaviour and it is able to produce accurate forecasts. In particular, the ground-truth CIR values are almost always within the predicted 95% confidence bands, thus providing a truthful interval in which the ground-truth CIR values are expected to lie.
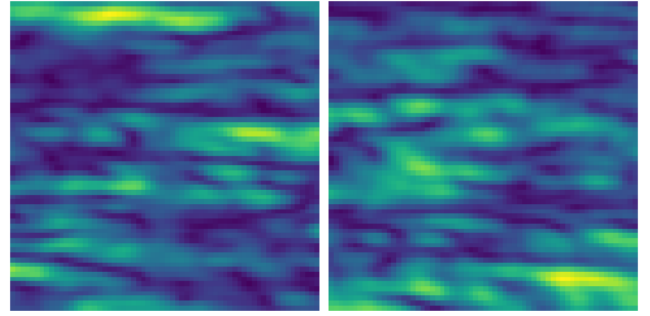
As exploratory future reseach, joint forecasting of multiple subcarriers can be investigated. In particular, leveraging on state-of-the-art attentional models [14], temporal correlations between different subcarriers can be exploited for producing more accurate forecasts, and for quantitatively evaluating the impact of each subcarrier in the output forecasts.

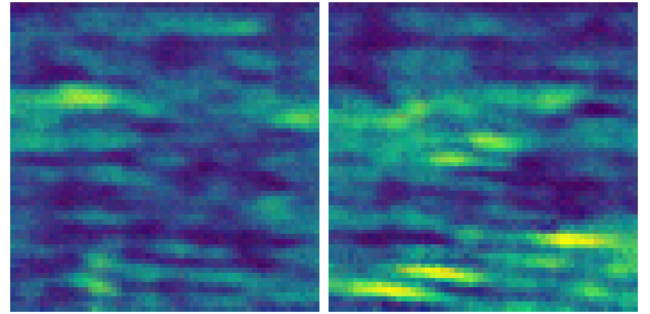### B. Channel Simulation with Generative Neural Networks

We consider the problem of building an approximate channel simulator given the measurement data. In other words, we aim at generating synthetic CTF samples whose behaviour over frequency and time resembles real measurements. Applications include the design of radio interfaces and systems in similar propagation environments, and benchmarking transmission and coding techniques in realistic, but diversified stochastic channel samples.

We propose leveraging on generative neural networks for building approximate channel models. The learning objective of generative neural networks is to model the distribution of a given dataset (in our case, CTF samples). Said distribution can then be cheaply sampled from, allowing for generating arbitrarily large volumes of new, synthetic data.

Leveraging on recent advances in synthetic generation of image data, we implement our generative network as a Deep Convolutional Generative Adversarial Network (DC-GAN) [15]. In particular, we consider the task of generating synthetic samples of the absolute CTF value over time and frequency. As such, we represent each experimental run in the presented dataset as a single image. At full resolution, each image will have height equal to the number of OFDM carriers, and width equal to the number of samples. For keeping training times reasonably short and facilitating convergence, we resize our input data down to 64x64.

Fig. 6 illustrates real and synthetic absolute CTF values for a center frequency of 2.55GHz and velocity equal to 40km/h. The synthetic CTF samples, albeit looking slightly noisy, are indeed visually resemblant to the real measurements. We underline that by leveraging off-the-shelf Graphical Processing Units (GPUs), large volumes of synthetic data can be generated in short computational times. Thus, our simple exercise illustrates the potential of generative neural networks for building realistic channel simulators.

V. CONCLUSION

In this paper, we describe the testbed hardware for collecting comparative time-varying channel measurements between sub-6 GHz and mmWave bands and we provide the corresponding measurement dataset. We outline in detail practical setup guidelines for ensuring the repeatability and the controllability of the experiments. After that, we describe the measurement campaign that has been conducted for creating the dataset. Finally, we present two illustrative ML use-cases for our dataset, namely CIR forecasting with recurrent neural networks and synthetic CTF generation with generative adversarial networks, and we suggest future exploratory research directions. Overall, our dataset provides rich dynamic channel measurements in highly diversified scenarios, thus enabling the development of innovative ML-driven methodologies on challenging real-world propagation environments. We hope

that the research community will find use and inspiration in our work.

REFERENCES

[1] J. Joo, M. C. Park, D. S. Han, and V. Pejovic, "Deep learning-based channel prediction in realistic vehicular communications," *IEEE Access*, vol. 7, pp. 27846–27858, 2019.

[2] C. Luo, J. Ji, Q. Wang, X. Chen, and P. Li, "Channel state information prediction for 5G wireless communications: A deep learning approach," *IEEE Transactions on Network Science and Engineering*, vol. 7, no. 1, pp. 227–236, 2020.

[3] Y. Teng, M. Liu, and M. Song, "Effect of outdated csi on handover decisions in dense networks," *IEEE Communications Letters*, vol. 21, no. 10, pp. 2238–2241, 2017.

[4] J. Connor, R. Martin, and L. Atlas, "Recurrent neural networks and robust time series prediction," *IEEE Transactions on Neural Networks*, vol. 5, no. 2, pp. 240–254, 1994.

[5] W. Jiang and H. D. Schotten, "Deep learning for fading channel prediction," *IEEE Open Journal of the Communications Society*, vol. 1, pp. 320–332, 2020.

[6] F. Pasic, S. Pratschner, R. Langwieser, D. Schützenhöfer, E. Jirousek, H. Groll, S. Caban, and M. Rupp, "Sub 6 GHz versus mmWave Measurements in a Controlled High-Mobility Environment," in *25th International ITG Workshop on Smart Antennas (WSA 2021)*, pp. 1–5, 2021. in press.

[7] F. Pasic, D. Schützenhöfer, E. Jirousek, R. Langwieser, H. Groll, S. Pratschner, S. Caban, S. Schwarz, and M. Rupp, "Comparison of Sub 6 GHz and mmWave Wireless Channel Measurements at High Speeds," in *16th European Conference on Antennas and Propagation (EuCAP 2022)*, pp. 1–5, 2022.

[8] S. Caban, J. Rodas, and J. A. García-Naya, "A methodology for repeatable, off-line, closed-loop wireless communication system measurements at very high velocities of up to 560 km/h," in *2011 IEEE International Instrumentation and Measurement Technology Conference*, 2011.

[9] M. Hofer, D. Löschenbrand, J. Blumenstein, H. Groll, S. Zelenbaba, B. Rainer, L. Bernadó, J. Vychodil, T. Mikulasek, E. Zöchmann, *et al.*, "Wireless Vehicular Multiband Measurements in Centimeterwave and Millimeterwave Bands," in *2021 IEEE 32nd Annual International Symposium on Personal, Indoor and Mobile Radio Communications (PIMRC)*, pp. 836–841, IEEE, 2021.

[10] V. Paliwal and I. Lambadaris, "Cell Search Procedures in LTE Systems," *Dept. Syst. Comput. Eng. Carleton Univ. Ottawa, ON, Canada, K1S 5B6*, pp. 1–6, 2005.

[11] B.-J. Choi, E.-L. Kuan, and L. Hanzo, "Crest-factor study of MC-CDMA and OFDM," in *50th Vehicular Technology Conference*, vol. 1, 1999.

[12] F. Pasic, "Multi-band wireless channel measurements in high-mobility environment, https://dx.doi.org/10.21227/3tpp-j394, IEEE Dataport," 2022.

[13] Y. Gal and Z. Ghahramani, "A theoretically grounded application of dropout in recurrent neural networks," in *Advances in Neural Information Processing Systems* (D. Lee, M. Sugiyama, U. Luxburg, I. Guyon, and R. Garnett, eds.), vol. 29, Curran Associates, Inc., 2016.

[14] B. Lim, S. O. Arık, N. Loeff, and T. Pfister, "Temporal fusion transformers for interpretable multi-horizon time series forecasting," *International Journal of Forecasting*, vol. 37, no. 4, pp. 1748–1764, 2021.

[15] A. Radford, L. Metz, and S. Chintala, "Unsupervised representation learning with deep convolutional generative adversarial networks," in *4th International Conference on Learning Representations, ICLR 2016, San Juan, Puerto Rico, May 2-4, 2016, Conference Track Proceedings* (Y. Bengio and Y. LeCun, eds.), 2016.

Faruk Pasic (Graduate Student Member, IEEE) received the Dipl.-Ing. degree (M.Sc. equivalent) from TU Wien, Austria, in 2021. He is currently pursuing the Ph.D. degree in telecommunications engineering with the Institute of Telecommunications, TU Wien. His main focus is on 5G vehicular-to-everything (V2X) communications.

Nicola Di Cicco (Graduate Student Member, IEEE) is currently working toward the Ph.D. degree with the Department of Electronic, Information, and Bioengineering, Politecnico di Milano, Milan, Italy. His research interests include deep learning and reinforcement learning for network optimization and automation.

Marco Skocaj (Graduate Student Member, IEEE) is currently working toward the Ph.D. degree with the Department of Electronic, Information and Electrical Engineering at the University of Bologna and WiLab, CNIT. He is chair of HA1 (Datasets) working group in COST action 20120 INTERACT. His research interests include Radio Resource Management, Machine Learning, Autonomous Networks and Optimization.

Massimo Tornatore (Senior Member, IEEE) is currently an Associate Professor with the Department of Electronics, Information, and Bioengineering, Politecnico di Milano. His research interests include performance evaluation, optimization and design of communication networks, network virtualization, network reliability, and machine learning application for network management.

Stefan Schwarz (Senior Member, IEEE) received the Dr. techn. degree (Ph.D. equivalent) in telecommunications engineering from TU Wien, Austria, in 2013. Since 2021, he is as an Associate Professor with the Institute of Telecommunications, TU Wien, where he also heads the Christian Doppler Laboratory for Dependable Wireless Connectivity. His research interests include wireless communications, signal processing, channel modeling and machine learning. He is an Associate Editor of IEEE Access, IEEE Communications Letters and EURASIP JWCN.

Christoph F. Mecklenbräuker (Senior Member, IEEE) received the Dipl.-(Ing.) degree (Hons.) in electrical engineering from TU Wien, Vienna, Austria, in 1992, and the Dr.-(Ing.) degree (Hons.) from Ruhr-Universität Bochum, Bochum, Germany, in 1998. Since 2006, he has been a Full Professor with the Institute of Telecommunications, TU Wien. His current research interests include 5G and 6G radio interfaces and antennas and propagation.

Vittorio Degli-Esposti (Senior Member, IEEE) is currently Associate Professor with the Department of Electrical Engineering of the University of Bologna and previously Director of Research at Polaris Wireless Inc., USA, in 2015-2016. He is Chair of the Propagation Working Group of the European Association on Antennas and Propagation (EurAAP) He is author or co-author of over 150 peer-reviewed technical papers and co-inventor of 7 international patents in the fields of applied electromagnetics, radio propagation and wireless systems.